


Silver hollandite ($\text{Ag}_x\text{Mn}_8\text{O}_{16}$, $x \leq 2$): A highly anisotropic half-metal for spintronicsFrancisco Sánchez-Ochoa ^{*}*Instituto de Física, Universidad Nacional Autónoma de México, Apartado Postal 20-364, Ciudad de México C.P. 01000, Mexico*Michael Springborg [†]*Physical and Theoretical Chemistry, University of Saarland, 66123 Saarbrücken, Germany* (Received 30 April 2021; revised 11 July 2021; accepted 11 August 2021; published 1 September 2021)

Structural, electronic, and magnetic properties of a crystalline material formed by parallel chains of silver atoms inside the tunnels of a manganese dioxide host with the hollandite structure, $\text{Ag}_x\text{Mn}_8\text{O}_{16}$, are studied with density functional theory (DFT) calculations. More magnetic structures were studied, including ferromagnetic (FM) and C2 antiferromagnetic (C2-AFM) orderings on Mn atoms of pristine hollandite Mn_8O_{16} and the FM state of $\text{Ag}_x\text{Mn}_8\text{O}_{16}$. Thereby, Hubbard corrections and different values for the Ag content, $x \leq 2$, were considered. The results show that hollandite Mn_8O_{16} is a semiconducting oxide both in the FM and in the AFM states, but with the C2-AFM configuration as the ground state. Interestingly, for the FM state of $\text{Ag}_x\text{Mn}_8\text{O}_{16}$ for high silver content, $x = 2$, the system is a perfect and isotropic half-metal, but when not all tunnels are filled with Ag chains, i.e., for $x < 2$, it behaves as a quasi-one-dimensional system retaining the perfect half-metallicity. The results demonstrate that the incorporation of the monoatomic Ag chains inside the hollandite Mn_8O_{16} host leads to a stable system that can be used as a spin filter for instance for spintronics devices.

DOI: [10.1103/PhysRevMaterials.5.095001](https://doi.org/10.1103/PhysRevMaterials.5.095001)

I. INTRODUCTION

Hollandite-type crystal structures containing transition-metal (TM = V, Cr, Mn, Mo, Ru, and Rh) atoms, i.e., the α -phase of TM_8O_{16} , have recently been the subject of intensive experimental and theoretical investigations [1–5]. The hollandite structure consists of octahedral units of corner- and edge-sharing TM oxides forming triangular ladders that are linked together and create one-dimensional square tunnels of a diameter around 4.7 Å. Hence, this porous host has enough space to accommodate small singly charged (Li^+ , Na^+ , K^+ , Rb^+ and Ag^+) [6] or doubly charged (Ba^{2+}) [7] cations. Thereby, the resulting material has potential applications in heterogeneous catalysis [8], as supercapacitors [9], and as cathode materials for rechargeable batteries [5,10] among others. In addition, from a fundamental point of view, these materials show interesting phenomena like orbital, charge, and spin ordering and phase transitions at low temperatures [11–17] and exotic topological properties as Weyl fermions at higher temperatures [18].

As an example we mention that at a critical temperature of $T_c \simeq 95$ K a metal-insulator transition (MIT) has been observed in Cr hollandite $\text{K}_2\text{Cr}_8\text{O}_{16}$ for which the FM ordering combined with an insulating behavior is stable [11,14]. As noticed by Hasegawa *et al.* [11], this is a rare case of a ferromagnetic insulator [12], whose existence otherwise has been associated with an instability ascribed to a Mott-Peierls mechanism [13]. Also the structural doubling of the unit cell

(“dimerization”) and the occurrence of a charge order accompanied by a structural distortion in hollandite $\text{K}_2\text{V}_8\text{O}_{16}$ have been studied [19], and the possibility that $\text{K}_2\text{Ru}_8\text{O}_{16}$ belongs to the class of Tomonaga-Luttinger liquids [15] has been discussed as well. Additionally, $\text{Ag}_2\text{Mn}_8\text{O}_{16}$ has been studied theoretically with several different approximate exchange-correlation functionals (including van der Waals interactions, Coulomb interactions through the GGA + U approach for Mn(3d) orbitals, the meta-GGA SCAN functional, and the hybrid HSE06 functional) [17] and predicted as being a metal for low Hubbard U values. However, for moderate values of $U = 3$ –5 eV an electron charge transfer mechanism from the Ag atoms to the hollandite leads to Mn^{3+} atoms, a charge localization, and an ordering in $\text{Ag}_2\text{Mn}_8\text{O}_{16}$, in agreement with results of HSE06 calculations. Indeed, a MIT in $\text{Ag}_2\text{Mn}_8\text{O}_{16}$ has been suggested earlier on the basis of DFT calculations [16] and very recently explored in experiments through transport properties at low temperatures [20].

Of relevance for the present work is that $\text{Ag}_x\text{Mn}_8\text{O}_{16}$ has been synthesized using a simple thermal process [21]. With this experimental approach, truncated octahedral silver nanoparticles are deposited on the surfaces of hollandite Mn_8O_{16} nanorods (HMO) and, subsequently, by means of a thermal treatment Ag atoms migrate along the external surface ($T = 383$ K) to the ends of the HMO, where a diffusion of the Ag atoms inside the HMO tunnels ($T \sim 493$ K) ultimately leads to the creation of single-atom Ag chains inside the parallel, squared-formed, quasi-one-dimensional tunnels [20]. It may be quite surprising that the procedure leads to essentially perfect chains of Ag atoms without vacancies or impurities. On the other hand, only a fraction of the tunnels may contain the silver chains. Thereby, the interactions between the

^{*}fsanchez@fisica.unam.mx[†]m.springborg@mx.uni-saarland.de

Ag chains are reduced and the systems become in effect of lower dimensionality. These systems are believed to have potential applications in nanocircuitry [20]. Motivated by these considerations, we study in this work the role of the silver content inside the HMO tunnels using DFT calculations on the properties of these materials, whereby we also will learn more about the guest-host interactions of the silver HMO systems. We emphasize already at this place that our results for $x = 2$ agree well with those of Kaltak *et al.* [17] but go beyond those by considering also $x < 2$.

Accordingly, in the present study, we report results of theoretical studies on the Ag-containing Mn_8O_{16} hollandite. We have used DFT calculations that include Coulomb and exchange interactions through the Hubbard term U_{eff} . In addition, we have varied the Ag content. We have studied the effects of the Coulomb and exchange interactions on the electronic and magnetic properties for spin-polarized C2-AFM of HMO and FM silver HMO structure. As we shall see, an interesting result is that the silver-containing HMO can act as a perfect spin filter.

II. METHODOLOGY

Collinear spin-polarized DFT calculations were performed using the Vienna *Ab initio* Simulation Package (VASP) [22] with the projector-augmented wave (PAW) method for describing the interactions between core and valence electrons [23]. The Perdew-Burke-Ernzerhof (PBE) parametrization within the generalized gradient approximation (GGA) for exchange and correlation effects was applied [24]. Structural parameters and forces were well converged using a Γ -centered $3 \times 3 \times 12$ Monkhorst-Pack grid [25] for the smallest $\text{Ag}_2\text{Mn}_8\text{O}_{16}$ unit cell and a 520 eV energy cutoff. A Gaussian smearing of 0.05 eV was used for the Fermi surface broadening. The optimization of atomic positions and lattice vectors were performed until residual forces were 10 meV/Å or less, and the electronic relaxation was converged to 10^{-8} eV.

Since HMO has Mn atoms with an open $3d$ shell a proper description of electron filling and magnetic moment of Mn atoms is needed to describe adequately the geometrical and electronic properties, including the electronic band gap, of HMO. To this end we study electronic correlations effects of Mn through the GGA + U_{eff} method, with $U_{\text{eff}} = U - J$, where U and J describe Coulomb and exchange interactions, respectively. Several values of U_{eff} and two approaches were studied to address the importance of U_{eff} on pristine HMO physical properties. We varied U_{eff} in steps of 1 eV in the range 0.9–6.9 eV since other reports have used near-integer [17,26–28] or integer values of U_{eff} [17,28] to describe the properties of HMO. We use the isotropic Hubbard term of Dudarev [29], hereafter called GGA + U_D , and the anisotropic Coulomb and exchange interactions within the Lichtenstein scheme [30], hereafter called GGA + U_L , with an atomic limit value of $J = 1.0$ eV as in Ref. [5] for the latter case. The second method is used since the importance of separate treatments of Coulomb and exchange interactions has previously been found to be important by Tompsett *et al.*, who studied the similar compounds $\beta\text{-MnO}_2$ [31] and HMO ($\alpha\text{-MnO}_2$) [5], and by Kaltak *et al.* on $\text{A}_2\text{Mn}_8\text{O}_{16}$ hollandite groups, where $A = \text{Ag, Li and K}$ [17].

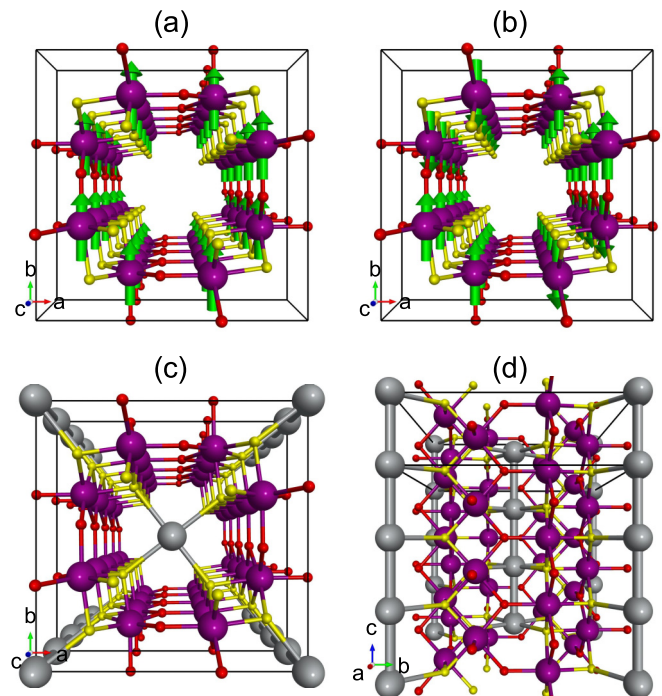


FIG. 1. Perspective top view of (a) FM and (b) C2-AFM ordering in pristine Mn_8O_{16} with green arrows denoting the spin alignment on Mn atoms. Perspective (c) top view and (d) side view of $\text{Ag}_2\text{Mn}_8\text{O}_{16}$. Color code: silver, purple, red, and yellow represent Ag, Mn, $\text{O}(\text{sp}^2)$, and $\text{O}(\text{sp}^3)$ atoms, respectively. The black line encloses the unit cell of a $1 \times 1 \times 4$ supercell.

Numerical calculations with the screened exchange hybrid functional, HSE06 [32] (25% of exact exchange and with $\omega = 0.2 \text{ \AA}^{-1}$) were taken as reference since the HSE06 functional has been found to describe better the electronic band gap of pristine HMO, the magnetic moment, and the magnetic ordering of the Mn atoms [17]. The same energy cutoff, k -point sampling and tolerance in residual forces and electronic optimization as mentioned above are used for these calculations. However, numerical calculations with the HSE06 functional have a high computational cost in comparison with the GGA + U_{eff} method which becomes problematic for larger HMO supercells with low Ag content. For this reason, the HSE06 calculations were used as a way to determine the best Hubbard method and U_{eff} value for the description of the electronic properties of the semiconducting HMO and then employ this GGA + U_{eff} approach to study larger $\text{Ag}_x\text{Mn}_8\text{O}_{16}$ supercells with reduced Ag content ($x < 2$).

III. RESULTS AND DISCUSSION

At first, we discuss the optimized crystal structures of pristine HMO using different approximations and magnetic orderings. All Mn atoms are in equivalent positions whereas there are two different types of O atoms, one forming edge-shared $\text{O}(\text{sp}^3)$ octahedra, while the other is forming corner-shared $\text{O}(\text{sp}^2)$ octahedra, see Fig. 1. Figures 1(a) and 1(b) show the FM and C2-AFM magnetic orderings on Mn atoms of HMO, respectively.

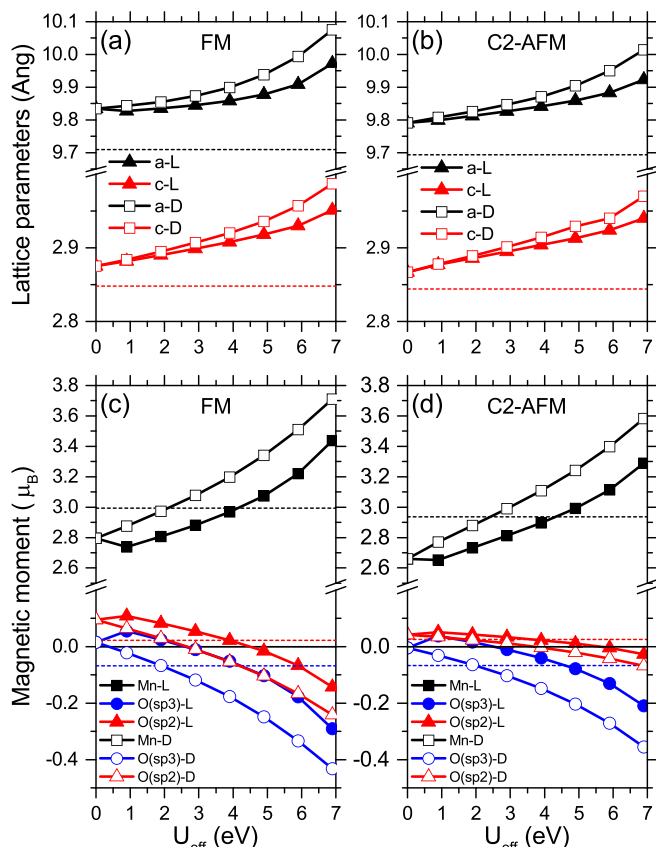


FIG. 2. Lattice parameters a and c as a function of the Hubbard U_{eff} value using the Lichtenstein (L) and the Dudarev (D) approaches for (a) the FM and (b) the C2-AFM ordering. The dashed black (red) line represents the calculated a (c) value using the HSE06 functional. (c) and (d) show the U_{eff} value dependence of the magnetic moments for a specific Mn atom and two neighboring O(sp³) and O(sp²) atoms for (c) the FM and (d) the C2-AFM magnetic ordering. The dashed black, red, and blue lines denote calculated magnetic moments using the HSE06 functional for Mn, O(sp³), and O(sp²) atoms, respectively.

The dependence of the GGA + U_{eff} method and Hubbard U_{eff} parameter on the lattice parameters, a and c , and the magnetic moments for specific Mn, O(sp³), and O(sp²) atoms of pristine HMO are depicted in Fig. 2. These results are compared with those calculated using the HSE06 functional in order to identify a proper U_{eff} value and method for pristine HMO. As can be seen in Figs. 2(a) and 2(b), the lattice parameters a and c increase as a function of U_{eff} for both the FM and the C2-AFM state. This implies an increase in the volume of the unit cell, see Fig. S1(a) of Supplemental Material (SM) [33], that can be related to an electron localization in Mn, O(sp³), and O(sp²) atoms in both magnetic FM and C2-AFM orderings, see Figs. 2(c) and 2(d). As for the lattice parameters, those calculated using the Lichtenstein method deviate less from the values using the HSE06 functional compared to those using the Dudarev approach as U_{eff} increases. Nevertheless, we have found two possible U_{eff} values for FM and C2-AFM orderings which properly describe well the magnetic moments of Mn and O atoms when comparing with the HSE06 results. These values are

$U_{\text{eff}} = 1.9$ eV for the Dudarev approach and $U_{\text{eff}} = 3.9$ eV for the Lichtenstein method. Notice that we have found that the C2-AFM regime is preferred for a lower U_{eff} value of $\simeq 4$ ($\simeq 6$) eV for the Dudarev (Lichtenstein) approach, whereas for larger U_{eff} values, the FM ordering is the more stable one; see Fig. S1(b) of SM [33]. This in-plane C2-AFM ordering of HMO has an FM coupling between nearest Mn atoms and an AFM coupling between adjacent Mn triangle ladders as discussed in detail in Refs. [16] and [27].

Based on previous reports [26,28] and on the results discussed above, we set $U_{\text{eff}} = 3.9$ eV as the optimal one. We shall now discuss the main differences in lattice parameters, relative energy between FM and C2-AFM state, magnetic moment of the Mn atoms, and the electronic band gap of the GGA, GGA + U_D , GGA + U_L , and HSE06 calculations. As shown in Table I, while the GGA + U_D method tends to overestimate the lattice parameters a and c , GGA and GGA + U_L give better results in comparison with the experimental values [34] and those calculated with HSE06. However, the relative energy of -19.74 meV/f.u. between the FM and the C2-AFM ordering as found with the GGA + U_L approach is comparable to -21.99 meV/f.u. of the HSE06 method. Similar values for the magnetic moments of $\simeq 3.0 \mu_B$ are found in all approaches, implying that the Mn ions have a Mn⁴⁺ ($3d^3$) valence state. Moreover, comparable magnetic moment differences between the C2-AFM and the FM state, i.e., $\sim 0.07 \mu_B$, are found too. The GGA + U_L approximation gives values for the electronic band gap of 1.63 eV (2.92 eV) for majority (minority) spin for the FM state, whereas GGA and GGA + U_D underestimate the value of the band gap. The values of the band gap for HMO with the FM or C2-AFM ordering as found with GGA + U_L are close to the experimental value of 2.23 eV [35], whereas HSE06 gives values of 2.96 eV (3.52 eV) for majority (minority) spin in the FM state as shown in Table I. A band gap value of 2.9 eV is obtained for the C2-AFM state with the HSE06 functional. In total, our calculated band gap values are in good agreement with those of other studies [1,2].

Figure 3 shows a clear increase of the band gap when passing from GGA to HSE06. In total, the GGA + U_L method with the Lichtenstein scheme [30] appears to give more accurate results for the C2-AFM ordering as the ground state and for the FM state of HMO instead when comparing with the results obtained when using the rotationally and invariant Hubbard term of Dudarev [29]. Furthermore, the FM DOS with GGA gives a band gap of $\lesssim 1$ eV with the majority (minority) spin forming the top (bottom) of the valence (conduction) band of the pristine HMO as shown in Fig. 3. Conversely, the FM DOS with the GGA + $U_{D,L}$ or the HSE06 functional result in a band gap with both the top of the valence band and the bottom of the conduction band coming from majority spin orbitals. From this analysis, we recognize the role of the U_{eff} parameter to describe correctly the FM and C2-AFM ordering and the electronic states around the Fermi level of pristine HMO.

The value $U_{\text{eff}} = 3.9$ eV of Dudarev in this work is consistent with the results by Noda *et al.* [28] according to which the energy difference between FM and C2-AFM orderings is almost zero for $U_{\text{eff}} \simeq 4.0$ eV; see Fig. S1(b) of SM [33]. Both for the FM and for the C2-AFM state of HMO, the HSE06 functional leads to Mn⁴⁺ ($3d^3$) configurations which is in good

TABLE I. Optimized lattice parameters a and c , relative energies E , magnetic moment of Mn μ , and electronic band gap GAP of pristine hollandite Mn_8O_{16} using different theoretical approaches, i.e., standard GGA ($U = J = 0$ eV), GGA+ U_D ($U = 3.9$ eV and $J = 0.0$ eV), GGA+ U_L ($U = 4.9$ eV and $J = 1.0$ eV), and the HSE06 functional, and for different ferromagnetic alignments, such as ferromagnetic (FM) and C2 antiferromagnetic (C2-AFM) orderings in Mn. The FM ordering is set as reference for the relative energy E . While FM orderings have different band gaps for majority (first value) and minority (second value) spin, the C2-AFM state has only one band gap as a consequence of symmetry.

	GGA		GGA+ U_D		GGA+ U_L		HSE06		Expt.
	FM	C2-AFM	FM	C2-AFM	FM	C2-AFM	FM	C2-AFM	
a (Å)	9.83	9.79	9.90	9.87	9.86	9.84	9.70	9.69	9.75 ^a
c (Å)	2.87	2.86	2.92	2.91	2.91	2.90	2.84	2.84	2.86 ^a
E (meV/f.u.) ^b	0	-72.52	0	-2.77	0	-19.47	0	-21.99	
μ (μ_B)	2.79	2.66	3.20	3.11	2.97	2.89	3.00	2.93	
GAP (eV)	0.91, 1.17	0.58	1.18, 2.91	1.54	1.63, 2.92	1.90	2.96, 3.52 ^c	2.90	2.23 ^d

^aData from Ref. [34].

^bRelative energy in meV per formula unit (f.u.) of MnO_2 .

^cData from Refs. [1] and [2].

^dData from Ref. [35].

agreement with the results of the GGA + U_L calculations with $U_{\text{eff}} = 3.9$ eV. For this reason plus the fact that structural parameters, such as lattice parameters and volume of HMO, and the relative energy difference between the C2-AFM and the FM states (see Fig. S1(b) of SM [33]) for GGA + U_L agree well with the results obtained with the HSE06 functional, we adopt the GGA + U_L method with $U_{\text{eff}} = 3.9$ eV to study $Ag_xMn_8O_{16}$ hollandite.

Next, we discuss the structural and electronic properties of the high-temperature FM phase of $Ag_2Mn_8O_{16}$ [16] that is shown in Figs. 1(c) and 1(d). The optimized structural parameters for the FM $Ag_2Mn_8O_{16}$, i.e., for the ground state are listed in Table S1 of SM [33]. In this case, the Ag^+ ions occupy four-coordinated sites binding to the $O(sp^3)$ atoms of

the tunnel walls instead of occupying an eight-coordinated site as found for other cations like K^+ , Rb^+ . This leads to a square-planar coordination of Ag^+ ions with $O(sp^3)$ atoms as the nearest neighbors [36]. Compared with the situation that the Ag atoms are placed at the 8-coordinated (Wyckoff 2b) site, this 4-coordinated (Wyckoff 2a) site is energetically favored by 0.5 eV/f.u. The calculated Ag-O(sp^3) bond lengths are 2.43 Å, 2.45 Å, and 2.45 Å for the GGA, GGA + U_D , and GGA + U_L calculations, respectively, whereas the Ag-Ag bond lengths are 2.87 Å, 2.99 Å, and 2.97 Å, respectively. The Ag-Ag nearest-neighbor distances are all equal and identical to the c lattice constant of HMO. As a consequence of this high symmetry, the Ag atoms form linear chains inside square HMO tunnels [20], see Fig. 1(c) and 1(d). The Ag atoms of the chains in adjacent tunnels are displaced by $c/2$ relative to each other along the tunnel direction.

In Fig. 4 we show the atom-resolved density of states (DOS) of FM $Ag_2Mn_8O_{16}$ as obtained using different calculational methods. At first, we observe that the FM $Ag_2Mn_8O_{16}$ system behaves as a metal with both majority and minority spin contributions crossing the Fermi level when using the GGA approximation, see Fig. 4(a). For the FM configuration, the magnetic moment of Mn, 2.57 μ_B as given in Table S1 (SM) [33], is lower than that of the pristine HMO, 2.79 μ_B , as given in Table I. On the other hand, when passing to the GGA + U_D and GGA + U_L approaches, FM $Ag_2Mn_8O_{16}$ becomes half-metallic with only majority spin contributions crossing the Fermi level and an electronic band gap greater than 2 eV for the minority spin, see Figs. 4(b) and 4(c). That only the majority spin crosses the Fermi level suggests that this material possesses a perfect spin-filtering effect, i.e., 100% spin-polarization ratio, with potential applications in spintronic devices. The total magnetic moments of the Mn atoms are 3.48 μ_B and 3.34 μ_B , see Table S1 (SM) [33], for GGA + U_D and GGA + U_L , respectively. These values are slightly greater than the magnetic moment of Mn in pristine HMO (Table I). The bands that cross the Fermi level either for both spin directions from the GGA calculations or for only the majority spin in the other calculations (see Figs. S2–S4 of SM [33]) have significant dispersion in all directions, indicating that the corresponding orbitals are delocalized over

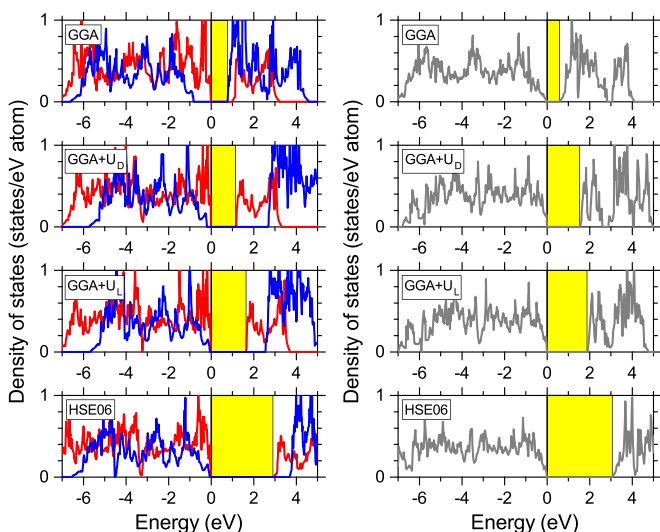


FIG. 3. Calculated density of states (DOS) for pristine hollandite Mn_8O_{16} as obtained with different theoretical approaches. The subscript D (L) denotes Dudarev (Lichtenstein) method. The left panels show the DOS with FM ordering. Majority and minority spins are plotted in red and blue, respectively. The right panels show the DOS of C2-AFM alignment. The yellow regions mark the electronic band gap, setting the Fermi level at the top of the valence bands.

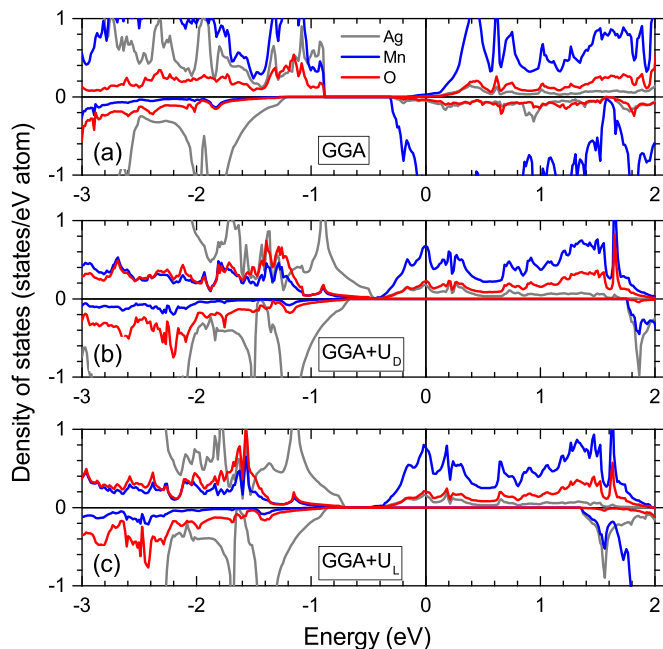


FIG. 4. Average atom-resolved densities of states (DOS) for FM $\text{Ag}_2\text{Mn}_8\text{O}_{16}$ using (a) GGA, (b) $\text{GGA} + U_D$, and (c) $\text{GGA} + U_L$. Positive (negative) DOS denotes majority (minority) spin. The black vertical line at 0 eV represents the Fermi level.

the complete system. Thus, the FM $\text{Ag}_2\text{Mn}_8\text{O}_{16}$ system behaves like a three-dimensional half-metal for $\text{GGA} + U_{D,L}$. Additionally, from Figs. 4(b) and 4(c) we can observe that Ag states form the top of the valence band meaning that the Ag^+ ions stabilize the HMO structure by bonding $\text{Ag-O}(sp^3)$ interactions. The electron transfer from Ag atoms to Mn atoms reduces Mn^{4+} to $\text{Mn}^{3.52+}$ and $\text{Mn}^{3.66+}$ for $\text{GGA} + U_D$ and $\text{GGA} + U_L$, respectively. The electronic and conductive properties of silver HMO are due to $3d$ orbitals of Mn in the triangular ladders. On the other hand, for the minority-spin direction, a sharp peak due to $\text{Ag}(5s)$ orbitals appears around +1.8 eV (+1.6 eV) for $\text{GGA} + U_D$ ($\text{GGA} + U_L$). This peak with a decaying behavior for higher energies has a one-dimensional character. Atom- and orbital-resolved DOS for FM $\text{Ag}_2\text{Mn}_8\text{O}_{16}$ with $U = 4.9$ eV and $J = 1.0$ eV are shown in Fig. 5, and they confirm that the metallic properties are due to the $\text{Mn}(3d)$ orbitals. $\text{Mn}(4s)$ and $\text{Ag}(5s)$ orbitals are empty and form the minimum of the conduction band for the minority spin. $\text{O}(2p_x, 2p_y)$ orbitals are degenerate in energy and participate in forming Ag-O bonds. The full band structure in Fig. S5 (SM) [33] shows that FM $\text{Ag}_2\text{Mn}_8\text{O}_{16}$ with maximum concentration of silver has three-dimensional conductive properties since at least one band (the blue one) crosses the Fermi level along all directions in reciprocal space. Therefore, this FM $\text{Ag}_2\text{Mn}_8\text{O}_{16}$ system is a three-dimensional perfect half-metal according to the $\text{GGA} + U_L$ calculations (which are the most accurate ones) with potential applications in spintronics as a spin filter.

Next we study the role of the silver content in $\text{Ag}_x\text{Mn}_8\text{O}_{16}$, $x \leq 2$. Keeping the Hubbard corrections at $U = 4.9$ eV and $J = 1.0$ eV (i.e., using the Lichtenstein method), the three additional structures with formulas $\text{Ag}_1\text{Mn}_8\text{O}_{16}$, $\text{Ag}_{0.5}\text{Mn}_8\text{O}_{16}$,

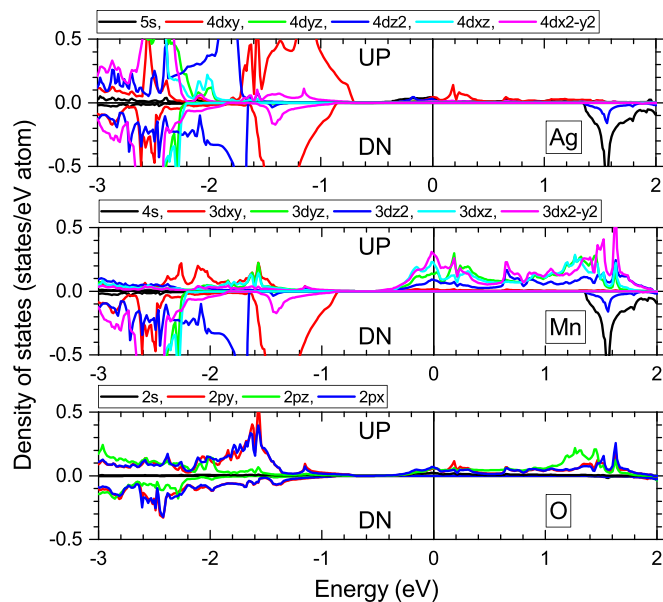


FIG. 5. Average atomic and orbital-resolved density of states (DOS) of FM $\text{Ag}_2\text{Mn}_8\text{O}_{16}$ with $\text{GGA} + U_L$ ($U = 4.9$ eV and $J = 1.0$ eV within the Lichtenstein method) for majority (UP) and minority (DN) spin contributions. The black vertical line at 0 eV represents the Fermi level.

and $\text{Ag}_{0.25}\text{Mn}_8\text{O}_{16}$ that are shown in Fig. S6 (SM) were studied [33]. These structures represent the case that only a single tunnel is occupied by an infinite Ag wire. When comparing the average atom-resolved DOS for $\text{Ag}_x\text{Mn}_8\text{O}_{16}$ with $x = 2$ shown in Fig. 4(c), i.e., $\text{GGA} + U_L$, with that for $x = 1$ shown in Fig. 6(a), we see that the sharp feature at the Fermi level for the majority spin for $x = 2$ becomes increasingly less pronounced for smaller x . This may not be surprising since the system with $x = 0$ is a semiconductor. The full band structure for FM $\text{Ag}_1\text{Mn}_8\text{O}_{16}$ in Fig. S7 (SM) [33] shows three bands crossing the Fermi level along the $\text{M} \rightarrow \text{A}$ direction whereas only one band does so along the $\Gamma \rightarrow \text{M}$, $\text{X} \rightarrow \Gamma$, and $\text{A} \rightarrow \text{Z}$ directions. This means that conduction is more favorable along the direction parallel to the Ag wires instead of the perpendicular directions and demonstrates that it is the presence of the Ag atoms that leads to a half-metallic state that is confined to the region closest to the Ag chain. Simultaneously, the minority $\text{Ag}(5s)$ states shift towards lower energies with decreasing Ag content. The inclusion of more empty tunnels in HMO when constructing larger supercells gives localized $\text{Ag}(4d)$ states in the valence regime. $\text{Mn}(3d)$ states in the conduction regime just above the Fermi level are confined to a narrow energy range which is due to the localized nature of these atomic orbitals. Whereas in Fig. 6(b) for $\text{Ag}_{0.5}\text{Mn}_8\text{O}_{16}$ the DOS takes an almost constant value around the Fermi level, that in Fig. 6(c) for $\text{Ag}_{0.25}\text{Mn}_8\text{O}_{16}$ possesses more sharp maxima, which is a manifestation of the quasi-one-dimensional behavior. Therefore, the combination of an accurate description of electron correlation and of the silver content in Ag-HMO results in a hybrid metallic-oxide nanostructure where the conductive properties are induced by but not confined to silver chains within an insulating TM oxide. The implications of this behavior in future electronic

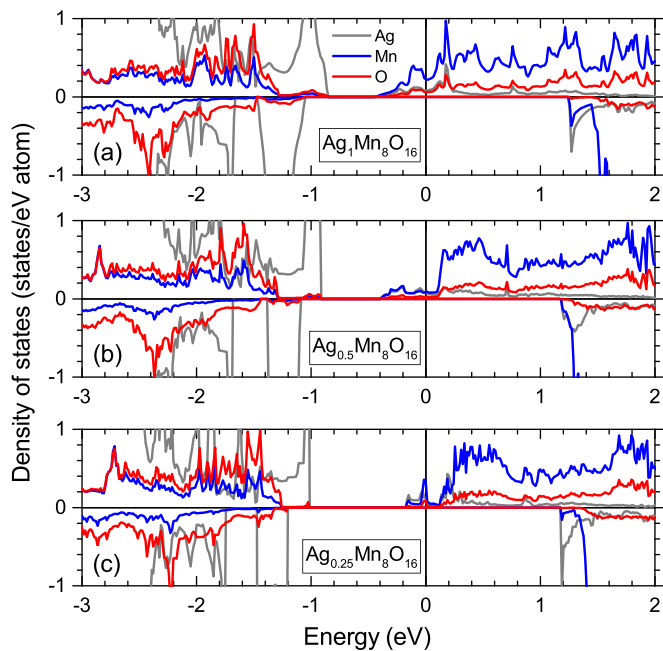


FIG. 6. Average atom-resolved densities of states (DOS) for FM Ag-HMO with GGA + U_L ($U = 4.9$ eV, $J = 1.0$ eV) and different silver concentrations: (a) $\text{Ag}_1\text{Mn}_8\text{O}_{16}$, (b) $\text{Ag}_{0.5}\text{Mn}_8\text{O}_{16}$, and (c) $\text{Ag}_{0.25}\text{Mn}_8\text{O}_{16}$. Positive (negative) DOS denotes majority (minority) spin. The black vertical line at 0 eV represents the Fermi level.

applications have been emphasized in Ref. [20], although that study did not include a full understanding of the guest-host interactions.

Finally, we shall discuss in more details the electronic structure of FM $\text{Ag}_{0.25}\text{Mn}_8\text{O}_{16}$ focusing on the orbitals in a small energy window around the Fermi level. The first Brillouin zone and its irreducible representation in blue are shown in Fig. 7(a) where high symmetry points are labeled. The band structure for the majority spin in the FM state is depicted in Fig. 7(b). As can be seen, the band structure is highly anisotropic with the largest dispersions parallel to the channels, $\Gamma \rightarrow Z$, implying that this direction is the preferred one for electron transport compared to the directions perpendicular to the silver chains, i.e., $\Gamma \rightarrow M \rightarrow X \rightarrow \Gamma$. Three bands, labeled B1, B2, and B3 cross the Fermi level of which B2 and B3 are degenerate. The B1 band covers the energy range from -0.2 eV to $+0.3$ eV. These three electronic bands are composed mainly of Ag($5s, 4d$) and Mn($3d$) orbitals, whereby the orbitals of the B1 band in the energy from -0.2 eV to the Fermi level are formed mainly by Ag($5s$) and Ag($4d_{z^2}$), cf. Fig. 7(c). In addition, the localized Mn($3d_{xz}, 3d_{yz}, 3d_{x^2-y^2}$) orbitals are most dominant closest to the Fermi level as shown in Fig. 7(d). It is worth mentioning that the partial DOS in Fig. 7(c) for the Ag($5s$) orbitals shows a behavior that is characteristic of one-dimensional systems. In order to prove the quasi-one-dimensionality of silver HMO with low Ag content plus Hubbard corrections in Mn atoms, we show the total electron density of the B1 and B2 bands in the (100)

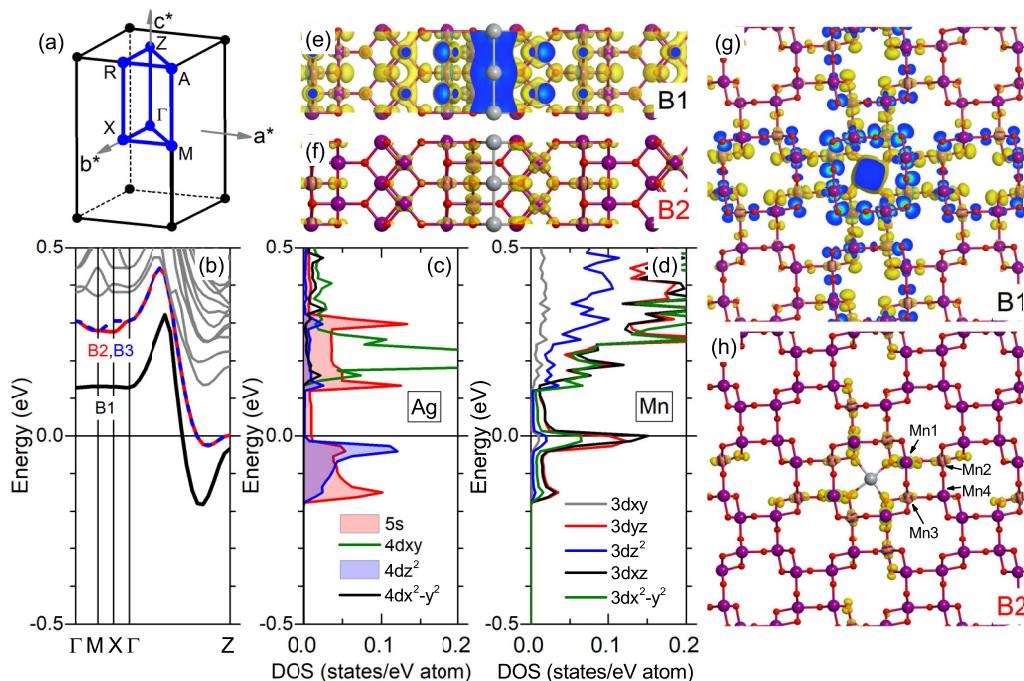


FIG. 7. Electronic properties of the FM $\text{Ag}_{0.25}\text{Mn}_8\text{O}_{16}$ system. (a) First Brillouin zone and its irreducible representation marked by the black and blue lines, respectively, as well as high symmetry points. (b) Energy band structure highlighting three bands B1 (black line), B2 (red line), and B3 (dashed blue line) crossing the Fermi level. The average atomic and orbital-resolved density of states (DOS) of (c) silver and (d) manganese atoms. (e) and (f) show the total electron density for bands B1 and B2 projected onto the (100) plane with majority (minority) spin plotted in yellow (cyan) with an isovalue of $10^{-4} e/\text{\AA}^3$, while (g) and (h) are projections onto the (001) plane. The labels M1–M4 in (h) denote Mn atoms with different charge and orbital ordering. Ag, Mn, and O atoms are represented by silver, purple, and red spheres, respectively. The Fermi level in (b), (c), and (d) is set to 0 eV.

plane in real space in Figs. 7(e) and 7(f), and projected onto the (001) plane in Figs. 7(g) and 7(h), that show isosurfaces of the density with majority (minority) spin represented by yellow (cyan). As can be seen from Figs. 7(e) and 7(g), a small amount of spin charge is localized to the O atoms, and a small delocalized density along the triangle ladders is found for the Mn atoms. The Ag atoms provide the major contribution of charge and spin delocalization constituting of spherical objects due to the $\text{Ag}(5s)$ states and a screened contribution from $\text{Ag}(4d_{z^2})$ orbitals. For the B2 band, shown in Figs. 7(f) and 7(h), we observe localized spin and charge densities on the Mn and O atoms in the closest vicinity of the Ag atoms without delocalization of charge along the tunnel of HMO. As shown in Fig. 7(h), four Mn atoms with different charge and orbital distribution can be identified. From Mn1 to Mn4 the charge decreases and, additionally, the DOS for Mn1 and Mn4 atoms have the same orbital distribution close to Fermi level being due to the $3d_{xz}$ orbital; see Fig. S8 of SM [33]. On the other hand, for the Mn2 and Mn3 atoms the $3d_{x^2-y^2}$ orbitals are almost completely filled. The charge ordering in Fig. 7(h) is similar to the CO4 ($\sqrt{2} \times \sqrt{2} \times 1$) ordering found by Kaltak *et al.* [17]. The B3 band shows a similar charge density in real space since B2 and B3 are degenerate. An analysis of the spin and charge densities of the B1 and B2 bands (Figs. S9–S11 of SM [33]) demonstrates that the Ag atoms are responsible for the conduction properties by means of the $\text{Ag}(5s)$ orbitals whereas the $\text{Ag}(4d_{z^2})$ orbitals are responsible for the interatomic bonds. In addition, we mention that the orbital ordering around the Fermi level of the Ag derived orbitals is consistent with the electronic structure of an isolated and periodic Ag chain, cf. Fig. S12 (SM) [33]. Therefore, using an accurate description of the system of our interest, including Hubbard corrections plus a precise control of the silver filling of HMO tunnels, allows us to predict that these materials are 100% spin polarized quasi-one-dimensional systems embedded inside the HMO tunnels. Indeed, since free-standing Ag chains are unstable, HMO represents an ideal host material to protect silver chains from external agents and thus to build atomic interconnections for spintronics devices.

To end, let us mention that Ag nanoparticles are placed on the surfaces of HMO in the experimental studies. Thereby, there is no control over the stoichiometry. Subsequently, the Ag atoms diffuse into the tunnels of the HMO and the re-

sulting $\text{Ag}_x\text{Mn}_8\text{O}_{16}$ system has an essentially arbitrary $x \leq 2$. This could suggest that the Ag atoms are placed randomly inside the tunnels of the HMO, which actually may be the case at elevated temperatures due to entropic effects. However, the experimental results demonstrate that the Ag atoms form perfect chains inside the tunnels of HMO which implies that only a fraction of all tunnels of HMO are completely filled with Ag chains. Thus, in this work we have constructed and studied systems based on these considerations.

IV. CONCLUSIONS

In summary, we have presented the electronic structure of silver hollandite $\text{Ag}_x\text{Mn}_8\text{O}_{16}$ using DFT with Hubbard corrections using two formalisms and different silver content, i.e., for $x \leq 2$. We reported results on the structural, electronic, and magnetic properties of the host material hollandite Mn_8O_{16} in both the ferromagnetic and the C2 antiferromagnetic state, and for the $\text{Ag}_x\text{Mn}_8\text{O}_{16}$ system in the ferromagnetic state. We found that the explicit inclusion of anisotropic Coulomb U and exchange J interactions enhances the electronic band gap and it improves the structural and electronic properties in comparison with experiment and with more sophisticated theories such as hybrid exchange-correlation functional. Most interesting is our finding that FM $\text{Ag}_x\text{Mn}_8\text{O}_{16}$ is a half-metallic system with 100% spin polarization with only contributions from the majority spin at the Fermi level, whereas an electronic band gap is obtained for the minority spin states. Furthermore, the silver content plays a crucial role since for low silver content, i.e., $x < 2$, the electronic properties around the Fermi level are due to $\text{Ag}(5s)$ and $\text{Ag}(4d_{z^2})$ states with a strong suppression of Mn($3d$) orbitals. At very low silver content, the $\text{Ag}_{0.25}\text{Mn}_8\text{O}_{16}$ system behaves as a perfect half-metal with quasi-one-dimensionality. Our results demonstrate the relevance of an accurate description of electron correlation anisotropically and provides an accurate description of the properties of silver chains inside a hollandite manganese oxide that should be relevant for future spin and electronic interconnections with low power dissipation.

ACKNOWLEDGMENTS

The authors thank Prof. X. Tang for suggesting this study and Dr. Z. Huang for fruitful discussions.

-
- [1] Y. Yuan, C. Zhan, K. He, H. Chen, W. Yao, S. Sharifi-Asl, B. Song, Z. Yang, A. Nie, X. Luo *et al.*, The influence of large cations on the electrochemical properties of tunnel-structured metal oxides, *Nat. Commun.* **7**, 13374 (2016).
 - [2] M. J. Young, A. M. Holder, S. M. George, and C. B. Musgrave, Charge storage in cation incorporated α - MnO_2 , *Chem. Mater.* **27**, 1172 (2015).
 - [3] L. Wu, F. Xu, Y. Zhu, A. B. Brady, J. Huang, J. L. Durham, E. Dooryhee, A. C. Marschilok, E. S. Takeuchi, and K. J. Takeuchi, Structural defects of silver hollandite, $\text{Ag}_x\text{Mn}_8\text{O}_y$, nanorods: Dramatic impact on electrochemistry, *ACS Nano* **9**, 8430 (2015).
 - [4] M. Özacar, A. S. Poyraz, H. C. Genuino, C.-H. Kuo, Y. Meng, and S. L. Suib, Influence of silver on the catalytic properties of the cryptomelane and ag-hollandite types manganese oxides OMS-2 in the low-temperature co oxidation, *Appl. Catal., A* **462-463**, 64 (2013).
 - [5] D. A. Tompsett and M. S. Islam, Electrochemistry of hollandite α - MnO_2 : Li-ion and na-ion insertion and Li_2O incorporation, *Chem. Mater.* **25**, 2515 (2013).
 - [6] J. Huang, A. S. Poyraz, S.-Y. Lee, L. Wu, Y. Zhu, A. C. Marschilok, K. J. Takeuchi, and E. S. Takeuchi, Silver-containing α - MnO_2 nanorods: Electrochemistry in Na-based battery systems, *ACS Appl. Mater. Interfaces* **9**, 4333 (2017).

- [7] A. M. Larson, P. Moetakef, K. Gaskell, C. M. Brown, G. King, and E. E. Rodriguez, Inducing ferrimagnetism in insulating hollandite $\text{Ba}_{1.2}\text{Mn}_8\text{O}_{16}$, *Chem. Mater.* **27**, 515 (2015).
- [8] P. Hu, Z. Huang, Z. Amghouz, M. Makkee, F. Xu, F. Kapteijn, A. Dikhtiarenko, Y. Chen, X. Gu, and X. Tang, Electronic metal-support interactions in single-atom catalysts, *Angew. Chem., Int. Ed.* **126**, 3486 (2014).
- [9] D. A. Tompsett, S. C. Parker, and M. S. Islam, Surface properties of $\alpha\text{-MnO}_2$: Relevance to catalytic and supercapacitor behaviour, *J. Mater. Chem. A* **2**, 15509 (2014).
- [10] E. M. Benbow, S. P. Kelly, L. Zhao, J. W. Reutenauer, and S. L. Suib, Oxygen reduction properties of bifunctional α -manganese oxide electrocatalysts in aqueous and organic electrolytes, *J. Phys. Chem. C* **115**, 22009 (2011).
- [11] K. Hasegawa, M. Isobe, T. Yamauchi, H. Ueda, J.-I. Yamaura, H. Gotou, T. Yagi, H. Sato, and Y. Ueda, Discovery of Ferromagnetic-Half-Metal-to-Insulator Transition in $\text{K}_2\text{Cr}_8\text{O}_{16}$, *Phys. Rev. Lett.* **103**, 146403 (2009).
- [12] P. Mahadevan, A. Kumar, D. Choudhury, and D. D. Sarma, Charge Ordering Induced Ferromagnetic Insulator: $\text{K}_2\text{Cr}_8\text{O}_{16}$, *Phys. Rev. Lett.* **104**, 256401 (2010).
- [13] S. Kim, K. Kim, and B. I. Min, Structural instability and the mott-peierls transition in a half-metallic hollandite : $\text{K}_2\text{Cr}_8\text{O}_{16}$, *Phys. Rev. B* **90**, 045124 (2014).
- [14] T. Toriyama, A. Nakao, Y. Yamaki, H. Nakao, Y. Murakami, K. Hasegawa, M. Isobe, Y. Ueda, A. V. Ushakov, D. I. Khomskii, S. V. Streltsov, T. Konishi, and Y. Ohta, Peierls Mechanism of the Metal-Insulator Transition in Ferromagnetic Hollandite $\text{K}_2\text{Cr}_8\text{O}_{16}$, *Phys. Rev. Lett.* **107**, 266402 (2011).
- [15] T. Toriyama, M. Watanabe, T. Konishi, and Y. Ohta, Quasi-one-dimensional electronic structure of hollandite ruthenate $\text{K}_2\text{Ru}_8\text{O}_{16}$, *Phys. Rev. B* **83**, 195101 (2011).
- [16] F. S. Ochoa, Z. Huang, X. Tang, G. H. Coccoletzi, and M. Springborg, Magnetostructural phase transition assisted by temperature in $\text{Ag-}\alpha\text{-MnO}_2$: A density functional theory study, *Phys. Chem. Chem. Phys.* **18**, 7442 (2016).
- [17] M. Kaltak, M. Fernández-Serra, and M. S. Hybertsen, Charge localization and ordering in $\text{A}_2\text{Mn}_8\text{O}_{16}$ hollandite group oxides: Impact of density functional theory approaches, *Phys. Rev. Materials* **1**, 075401 (2017).
- [18] J. Z. Zhao, Y. J. Jin, R. Wang, B. W. Xia, and H. Xu, Weyl fermions in ferromagnetic high-temperature phase of $\text{K}_2\text{Cr}_8\text{O}_{16}$, *New J. Phys.* **22**, 073062 (2020).
- [19] A. C. Komarek, M. Isobe, J. Hemberger, D. Meier, T. Lorenz, D. Trots, A. Cervellino, M. T. Fernández-Díaz, Y. Ueda, and M. Braden, Dimerization and Charge Order in Hollandite $\text{K}_2\text{V}_8\text{O}_{16}$, *Phys. Rev. Lett.* **107**, 027201 (2011).
- [20] Y. Chen, D. Tang, Z. Huang, X. Liu, J. Chen, T. Sekiguchi, W. Qu, J. Chen, D. Xu, Y. Bando *et al.*, Stable single atomic silver wires assembling into a circuitry-connectable nanoarray, *Nat. Commun.* **12**, 1191 (2021).
- [21] Z. Huang, X. Gu, Q. Cao, P. Hu, J. Hao, J. Li, and X. Tang, Catalytically active single-atom sites fabricated from silver particles, *Angew. Chem., Int. Ed.* **51**, 4198 (2012).
- [22] G. Kresse and J. Furthmüller, Efficient iterative schemes for ab initio total-energy calculations using a plane-wave basis set, *Phys. Rev. B* **54**, 11169 (1996).
- [23] G. Kresse and D. Joubert, From ultrasoft pseudopotentials to the projector augmented-wave method, *Phys. Rev. B* **59**, 1758 (1999).
- [24] J. P. Perdew, K. Burke, and M. Ernzerhof, Generalized Gradient Approximation Made Simple, *Phys. Rev. Lett.* **77**, 3865 (1996).
- [25] H. J. Monkhorst and J. D. Pack, Special points for brillouin-zone integrations, *Phys. Rev. B* **13**, 5188 (1976).
- [26] C. Ling and F. Mizuno, Capture lithium in $\alpha\text{-MnO}_2$: Insights from first principles, *Chem. Mater.* **24**, 3943 (2012).
- [27] Y. Crespo and N. Seriani, Electronic and magnetic properties of $\alpha\text{-MnO}_2$ from ab initio calculations, *Phys. Rev. B* **88**, 144428 (2013).
- [28] Y. Noda, K. Ohno, and S. Nakamura, Momentum-dependent band spin splitting in semiconducting MnO_2 : A density functional calculation, *Phys. Chem. Chem. Phys.* **18**, 13294 (2016).
- [29] S. L. Dudarev, G. A. Botton, S. Y. Savrasov, C. J. Humphreys, and A. P. Sutton, Electron-energy-loss spectra and the structural stability of nickel oxide: An LSDA+U study, *Phys. Rev. B* **57**, 1505 (1998).
- [30] A. I. Lichtenstein, V. I. Anisimov, and J. Zaanen, Density-functional theory and strong interactions: Orbital ordering in Mott-Hubbard insulators, *Phys. Rev. B* **52**, R5467(R) (1995).
- [31] D. A. Tompsett, D. S. Middlemiss, and M. S. Islam, Importance of anisotropic coulomb interactions and exchange to the band gap and antiferromagnetism of $\beta\text{-MnO}_2$ from DFT+U, *Phys. Rev. B* **86**, 205126 (2012).
- [32] J. Heyd, G. E. Scuseria, and M. Ernzerhof, Hybrid functionals based on a screened coulomb potential, *J. Chem. Phys.* **118**, 8207 (2003).
- [33] See Supplemental Material at <http://link.aps.org/supplemental/10.1103/PhysRevMaterials.5.095001> for U_{eff} dependence of unit cell volume and relative energy between FM and C2-AFM orderings. Table with structural data of hollandite $\text{Ag}_2\text{Mn}_8\text{O}_{16}$ in FM state. DOS and band structures for $\text{Ag}_2\text{Mn}_8\text{O}_{16}$ with different approximations. Full band structure for FM $\text{Ag}_2\text{Mn}_8\text{O}_{16}$. $\text{Ag}_x\text{Mn}_8\text{O}_{16}$ supercell models with different Ag content, $x < 2$. Full band structure for FM $\text{Ag}_1\text{Mn}_8\text{O}_{16}$ with GGA + U_L (Lichtenstein scheme). Charge and orbital ordering in Mn atoms near Ag. Partial (band decomposed) charge density of bands along the (100) and (001) planes and electronic structure of periodic Ag chain.
- [34] C. Johnson, D. Dees, M. Mansuetto, M. Thackeray, D. Vissers, D. Argyriou, C.-K. Loong, and L. Christensen, Structural and electrochemical studies of α -manganese dioxide ($\alpha\text{-MnO}_2$), *J. Power Sources* **68**, 570 (1997), Proceedings of the Eighth International Meeting on Lithium Batteries.
- [35] N. Sakai, Y. Ebina, K. Takada, and T. Sasaki, Photocurrent generation from semiconducting manganese oxide nanosheets in response to visible light, *J. Phys. Chem. B* **109**, 9651 (2005).
- [36] F. M. Chang and M. Jansen, $\text{Ag}_{1.8}\text{Mn}_8\text{O}_{16}$: Square planar coordinated Ag^{II} ions in the channels of a novel hollandite variant, *Angew. Chem., Int. Ed. in English* **23**, 906 (1984).